Solar Energy Materials & Solar Cells 246 (2022) 111935

Contents lists available at ScienceDirect

Solar Energy Materials and Solar Cells

journal homepage: www.elsevier.com/locate/solmat

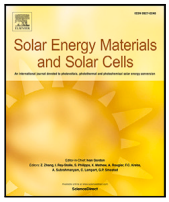

Random subwavelength structures on glass to improve photovoltaic module performance

Cristina L. Pinto [a,b,*], Iñaki Cornago [a], Alicia Buceta [a], Eugenia Zugasti [a], Jaione Bengoechea [a]

[a] National Renewable Energy Centre (CENER), C/ Ciudad de la Innovación 7, Sarriguren, 31621, Navarra, Spain
[b] Institute of Smart Cities (ISC), Public University of Navarra (UPNA), Campus Arrosadia, Pamplona, 31006, Navarra, Spain

ARTICLE INFO

Keywords:
Photovoltaic glass
Subwavelength structures
Anti-reflective
Anti-soiling
Super-hydrophilic
Solar cells

ABSTRACT

Glass samples have been processed by a single-step self-masking RIE (Reactive Ion Etching) process to obtain random subwavelength structures (SWSs), which mimic anti-reflective and anti-soiling patterns present in nature. The SWSs fabricated on glass provide an excellent broadband omnidirectional anti-reflective (AR) property (<1% absolute reflectance) in the spectral region (300–1200) nm due to the graded refractive index that these SWS produce in the air–glass interface, reducing the reflectance. Moreover, these SWSs increase the roughness of the glass surface enhancing its wettability and anti-soiling properties. In order to quantify the performance improvement of photovoltaic devices when using these structured glasses as front cover, commercial PERC (Passivated Emitter and Rear Contact) solar cells have been laminated with these structured glasses using the standard configuration (glass/EVA/Solar Cell/EVA/backsheet) and their electrical parameters such as I–V curve, spectral response, and IAM (Incidence Angle Modifier) factor have characterized.

1. Introduction

The energy that comes from the Sun sustains life on Earth. Its energy allows plants to carry out photosynthesis, warms our bodies, creates air-pressure differences in the atmosphere and promotes the water and many other chemical circles. Solar energy, being an inexhaustible and renewable energy source, can be harvested in different ways to produce electrical or thermal energy. Wind, biomass, and solar technologies are renewable energy technologies that convert direct or indirect solar energy into useable energy. Among them, solar PV is a mature technology that directly converts incoming photons from the Sun into electricity and has become the most important source of renewable energy nowadays. In fact, the total cumulative installed capacity of PV at the end of 2020 reached 760.4 GW_{dc} which covered 3.7% of the world's electricity generation [1].

Nowadays, there are many types of PV technologies. Most of them (almost 95% [2,3]) are based on silicon, however, other technologies such as thin-film, multi-junction, and emerging PV technologies are also being researched and installed. Although their technological basis is different, the majority use glass as a front cover and their efficiency can also be affected by the front cover glass. Apart from PID (Potential Induced Degradation) and absorption, there are two main reasons connected to PV glass than can decrease the efficiency of a solar module, i.e. reflection and soiling.

Soda-lime is a clear low-iron glass, widely used in the PV industry. It protects solar cells against atmospheric agents, provides strength, and determines light transmission properties. However, due to the refractive index mismatch between air (n=1) and glass (n=1.51), approximately 4% of the incident light is reflected at this first interface. To overcome this problem, nowadays, AR coatings are added to this first interface to increase the transmittance around 3% in absolute [4]. AR coatings reduce the reflection through destructive interference, following the quarter-wave principle [5]. To achieve this behaviour, AR coatings need to have a refractive index between glass and air. For this reason, most of these AR coatings are based on porous dielectric materials, like silica (SiO_2), alumina (Al_2O_3), and titania (TiO_2) deposited by sol–gel [6–9]. However, this strategy is only effective for a narrow range of wavelengths and incidence angles, out of these conditions, the efficiency of these AR coatings decreases.

On the other hand, soiling refers to the accumulation of dust, soil, organic materials, or other particles on PV module's front glass. When these dust particles settle on the glass, they cover the surface, reducing the amount of light that reaches the solar cell and decreasing, therefore, the power output. In fact, in regions where the solar resource is more abundant, i.e. in the Sun's Belt, normally the soiling rate also increases [10,11]. Even though this soiling rate might depend on the location, environmental conditions and tilt angle of the module, in

* Corresponding author at: Institute of Smart Cities (ISC), Public University of Navarra (UPNA), Campus Arrosadia, Pamplona, 31006, Navarra, Spain.
E-mail address: cristinaleyre.pinto@unavarra.es (C.L. Pinto).

https://doi.org/10.1016/j.solmat.2022.111935
Received 24 February 2022; Received in revised form 28 July 2022; Accepted 29 July 2022
Available online 11 August 2022

arid regions like deserts, the transmittance can be reduced up to 60% in a month [12–18]. To overcome this issue, wettability enhanced (WE) coatings are recently being developed and added to solar front cover glasses. This behaviour is achieved through hydrophobicity or hydrophilicity, either by increasing the roughness of the surface or changing the surface's free energy by chemicals.

To solve these challenges, new and more advanced biomimetic coatings and structures have received more attention lately. Nature, through millions of years of evolution, has developed optimal structures to achieve AR and WE behaviours. Cicada's or Greta Oto butterfly's transparent wings, super AR moth eyes, super-hydrophobic lotus leaves, shark skin are examples of functionalized structures present in nature [8,19–25]. These functionalities are given by subwavelength or hierarchical structures. Using the nature knowledge, several researchers have applied SWS to PV technology. Jeasung Son et al. [26–28] created randomly distributed nanostructures on glass surface to increase its transmittance and self-cleaning effect and they applied these glasses to PV technology. In this case, the SWS fabrication of nano-pillars consisted of a multi-step process including Ni deposition, annealing, dry etching, and remaining Ni particle removal, after which a chemical functionalization was carried out. They demonstrated an improvement in the glass transmittance averaged from 600 nm to 1200 nm of approximately 2%, and monitored the glass samples outdoors during 3 months, to conclude that the effects are pronounced in the case of superhydrophilic surfaces (without any further surface chemical treatment), compared to hydrophobic, superhydrophobic and hydrophilic surfaces. In these articles, in order to determine the electrical improvement, the nanostructured glasses were placed directly above the solar cells. The final lamination process with a solar cell, which allows quantifying the performance improvement of industrial photovoltaic devices when using these structured glasses as the front cover, was missing. On the other hand, Jorik van Groep et al. [29] coated borosilicate glass samples with periodic silica nanostructures, based on sol–gel chemistry and large area substrate-conformal soft-imprint technology. The printed 120 nm tall silica nano-cylinders provided an anti-reflection coating that reduced the double-side reflection from 7.35% to 0.57% (averaged over the visible spectral range). When laminating these coated glasses (3 mm-thick low-iron glass side at the front) with small solar cells (5×5 cm^2) in the standard configuration they measured a relative increase in the short circuit current of 3.8%. In this case, the durability of this silica coating against outdoor conditions and abrasion procedures shall be demonstrated. Monolithic structures have potentially better performance in terms of durability in comparison with coatings [30,31].

In this work, we present optimized random nanocones fabricated on glass surfaces by a simple and controllable one-step self-masking RIE process. These nanostructures improve the broadband and omnidirectional anti-reflective property, provide wettability enhancement and anti-soiling behaviour to the glass without using multiple fabrication procedures. It has been experimentally confirmed that this surface patterning enhances the electrical output of solar devices laminated with these glasses, potentially reducing operation and maintenance costs, and increasing the reliability of the whole PV system. First, the fabrication procedure of glasses with different structures will be described joined with their results in terms of spectral reflectance and transmittance, corresponding to Section 3.1. Afterwards the wettability and anti-soiling functionalities of the structured glasses have been analysed in Section 3.2 and Section 3.3 respectively. Finally, in Section 3.4, to the aim of quantifying the performance improvement of photovoltaic devices when using these structured glass as the front cover, commercial PERC (Passivated Emitter and Rear Contact) solar cells have been laminated with these structured glass using the standard configuration (glass/EVA/Solar Cell/EVA/backsheet) and their electrical parameters such as I–V curve, spectral response and IAM (Incidence Angle Modifier) factor have been carefully characterized.

2. Methods and materials

Borofloat® 33 glass samples have been structured with optimum nano-sized random cones on their surfaces. First of all, the anti-reflective property has been simulated to obtain the optimum structure [32].

After a standard cleaning procedure, glass substrates have been structured by means of Meyer Burger's (previously Roth & Rau) AK400 RIE system. Gas flow, gases composition (different mixtures of CF_4, SF_6, O_2 and Ar), process time, DC Bias voltage and chamber pressure have been varied in order to optimize the formation of SWSs. The surface topology images of etched glasses have been obtained by means of a Hitachi S-4700 Electron Microscope (SEM).

To characterize the anti-reflective property, the global, diffuse, and direct spectral reflectance and the global spectral transmittance from 300 nm to 1600 nm have been measured by means of a spectrophotometer (Instrument Systems). Moreover, direct reflectance at different light incident angles has been measured by means of Perkin Elmer's UV–Vis–NIR spectroscopy Lambda 1050 using the Universal Reflectance Accessory.

For the wettability effect, water contact angle (WCA) measurements have been carried out with a CAM 100 contact angle goniometer (CAM 100, KSV Instruments, Burlington, VT, USA) using distilled water. Results have been calculated using the average of the measurements and their standard deviations. Moreover, to characterize the self-cleaning property, half a glass sample has been structured and the sliding angle in each half has also been measured using 20 μL of DI water.

To characterize the anti-soiling effect, an indoor procedure, shown in Fig. 1, has been specifically developed to compare the adherence of soiling to structured glasses in comparison with flat glass.

This basic procedure consists in several steps. First, using a 4-digit scale, the glass samples have been weighed. A hermetic domed chamber (Fig. 2a), with an input port, has been modified adding a 3D printed spoon right below the input port (Fig. 2b). In this spoon, 0.5 g of standardized Arizona test Dust A2 have been deposited before the samples placement to prevent pre-soiling of the samples. After the chamber has been closed, a pressurized N_2 gun has been inserted and triggered from the input port. This N_2 shot disperses the dust throughout the domed chamber evenly, settling on all samples equally. Once the deposition has been finished, the samples have been weighed again in order to characterize the homogeneity of dust deposition. Next, for the dust removal, all samples have been vertically placed in a sample holder (Fig. 2c) and it has been tapped five times in order to allow the elimination of non-adhered dust. This procedure ensures that all samples undergo the same dust removal process, guaranteeing the homogeneity and repeatability of the experiment. The samples have been finally weighed again to obtain the adhered dust mass.

After these dust deposition step, the dust adhesion has been quantified by means of three different measurements procedures:

- First, the adhesion of the dust particles to the glass can be quantitatively measured by relating the weight of adhered dust and the deposited dust. The adhesion can be obtained by the following Eq. (1):

$$Adhesion(\%) = \frac{Adhered\ dust}{Deposited\ dust} \times 100 \quad (1)$$

- Alternatively, the soil surface covering ratio has also been measured by means of optical microscopy and an image processing program (FIJI).
- Finally, the transmittance has been measured by spectrophotometry to quantify the reduction of this parameter after the soiling process.

After the complete characterization of the structured glass samples, they were used as a front cover for solar PV mini-modules. Commercial

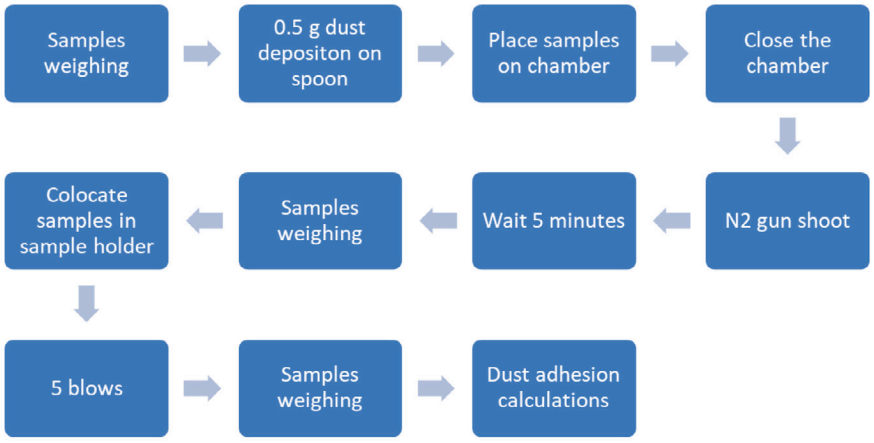

Fig. 1. Route of the anti-soiling characterization procedure.

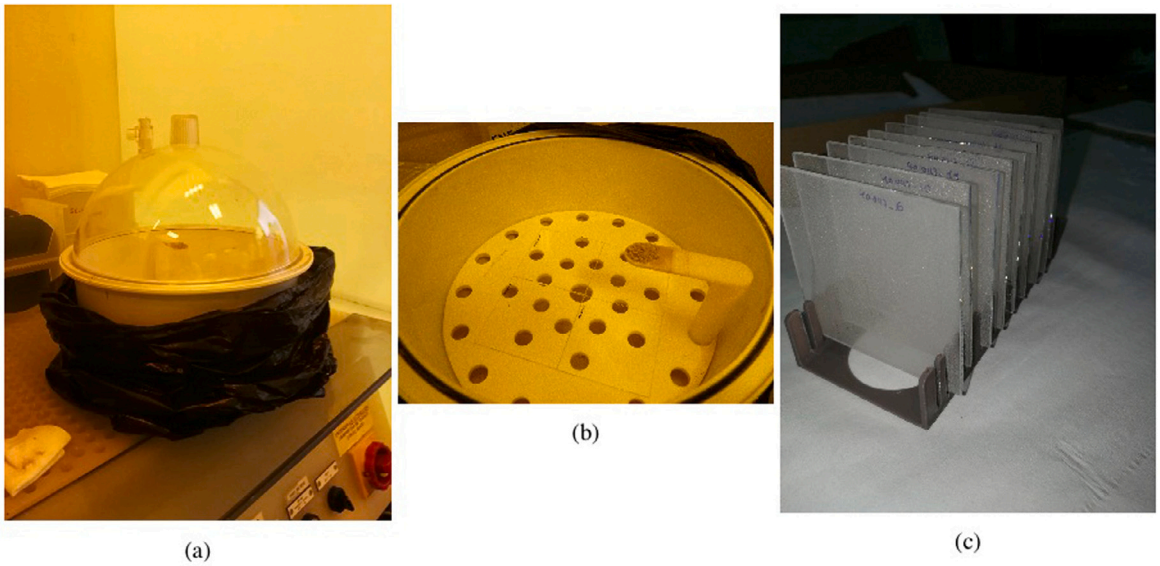

Fig. 2. (a) Hermetic domed chamber, (b) chamber with test dust in the spoon, (c) sample holder with dirty samples.

monocrystalline passivated emitter rear cells (PERC) have been laminated using ethyl-vinyl-acetate (EVA) as encapsulant and TEDLAR® as back-sheet. This process has been performed with a Laminator L036 A, from P. Energy SRL, using a standard lamination procedure.

Once laminated, the reflectance of the mini-modules has been measured with the spectrophotometer. Besides, the spectral response has been obtained by means of a Spectra-Nova Spectral Response SN SR-XS130-1 system. The photogenerated minimodule's electrical parameters have been measured using accredited testing laboratory equipment (Solar Flash Simulator Illb from Pasan S. A.). As an additional parameter, the response of the minimodules laminated with structured glasses with respect to the light's angle of incidence has been obtained applying the IAM factor (2) procedure following the normative IEC 61853-2 Ed. 1.0 [33]. With this aim, the short circuit current (Isc) has been measured with steps of 5 degrees using an angle changing tool (Fig. 3) by means of the above described Solar Flash Simulator:

$$IAM = \frac{I_{sc}(\theta)}{I_{sc}(0) \times cos\theta} \quad (2)$$

3. Results and discussion

3.1. Optical response

The nanocones are defined as SWSs since the distance between adjacent motifs is smaller than the shortest light wavelength and therefore, no light diffraction is produced. These SWSs act as an effective layer with refractive index gradually changing from n=1 (air) to n=1.48 (borosilicate glass), as shown in Fig. 4, effectively suppressing the reflection in this interface and showing a broadband anti-reflective property.

According to our previous study [32], a nanocone average height ($\bar{h}$) of 250 nm is enough to achieve a solar weighted reflectance lower than 0.5% at the first glass–air interface. However, different structures with a wide range of average heights and average heights' standard deviations (σ_h) have been fabricated to analyse the effect of these structures on the performance of PV devices and their applicability to solar PV technology. Table 1 shows the average height and the average peak to peak distance between adjacent nanostructures.

The global spectral transmittance and reflectance of structured glass samples have been measured and compared to a flat glass and a

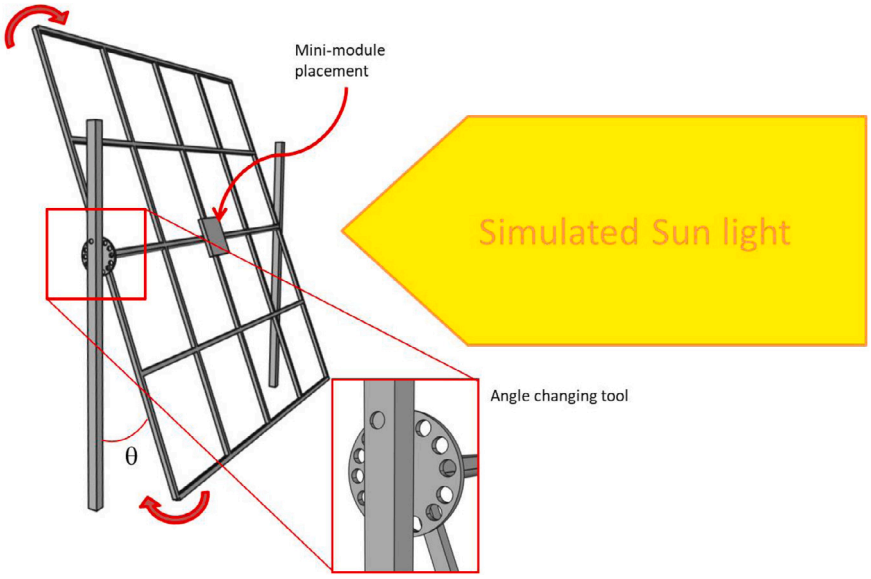

Fig. 3. IAM factor measurements set-up.

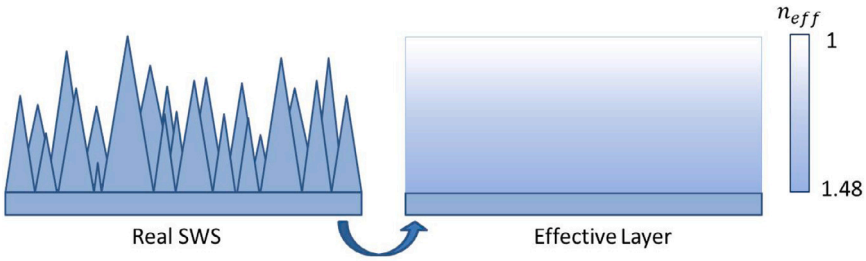

Fig. 4. Scheme of the effective layer with gradual refractive index.

Table 1
Topological parameters of structured glass samples.

Sample name	Structured sides	Average height (nm)	Peak to peak distance (nm)
Flat glass	–	–	–
Sample 1	One side	200	111
Sample 2	One side	243	119
Sample 3	Double side	243	119
Sample 4	One side	658	228

commercial photovoltaic glass with AR coating. To prove the homogeneity of the structures, the reflectance spectral measurements have been taken in 5 different locations on the samples, showing nearly the same spectra, with differences in the range of 0.01%. Fig. 5 shows the spectral transmittance of all the structured glasses described in Table 1, along with the convoluted spectral solar irradiance ($E_{conv}(\lambda) = SR(\lambda) \times E_{AM1.5}(\lambda)$, where $SR(\lambda)$ is the spectral response of a commercial PERC solar cell, and $E_{AM1.5}$ is the standard AM1.5 solar irradiance). As it can be comprehended from Fig. 5, modifying the nanocone's average height, the spectral transmittance can be controlled, acting on specific spectral region. As the average height increased, the wavelength region where the transmittance is higher shifts towards infrared regions. For Sample 1, the transmittance peak wavelength was located around 500 nm, for Sample 2 and Sample 3 their peak was around 600 nm, and for Sample 4, it was presumably out of the range. It has to be mentioned that Sample 4 could not be considered as SWSs for visible light since its nanocones' peak to peak distances is higher than the requirement $d_{SWS} < \frac{\lambda}{2n_{glass}}$.

In order to show the optical potential of structures from Sample 2, this same structures have been fabricated on the front and rear sides of another glass sample (Sample 3). These nano-structures presented a higher transmittance than a flat glass and a commercial PV glass with AR coating. More specifically, the transmittance averaged in the spectral region from 300–1200 nm increases 2.7% and 5.6% absolute compared to flat glass, for Sample 2 and Sample 3 respectively. Taking into account crystalline silicon PV performance, these nano-structures were identified as the best option among the studied structures as their equivalent short-circuit current density was the highest. For this reason, only these nano-structures will be analysed from now on. This parameter was calculated through the next Eq. (3):

$$J_{esc} = \sum_{\lambda=300nm}^{\lambda=1200nm} T(\lambda) \times SR(\lambda) \times E_{AM1.5}(\lambda) \quad (3)$$

where J_{esc} is the equivalent short-circuit current density, T is the glass transmittance, SR is a commercial PERC solar cell spectral response and E is the standard AM1.5 solar irradiance.

In order to complete the optical characterization, the spectral reflectance of the optimum nano-structure was also measured. As it can be seen from Fig. 6(a), one side structured glass showed an anti-reflective property, with a decrease of 3.0% absolute with respect to a flat glass, exhibiting only 4.1% reflectance averaged in the spectral region from 300 nm to 1200 nm. Moreover, structuring both sides of

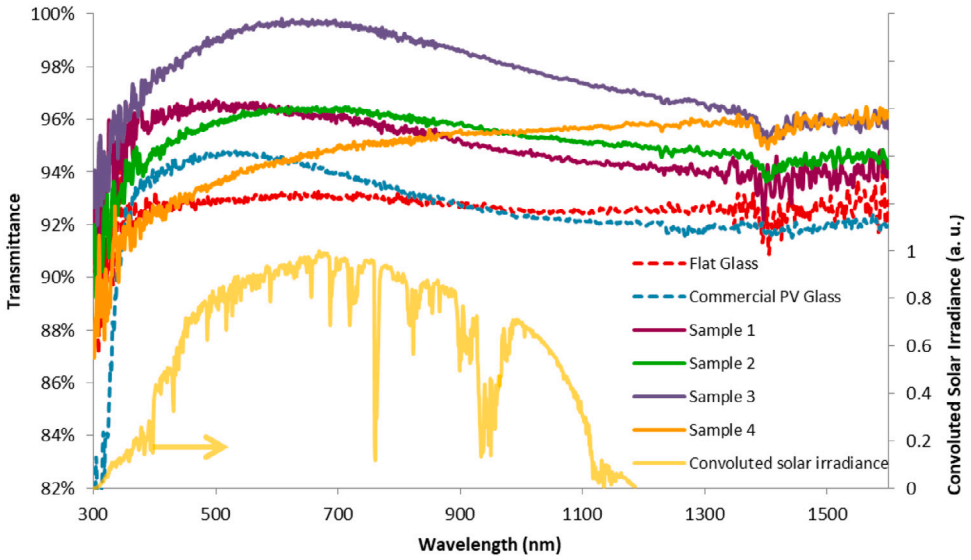

Fig. 5. Spectral transmittance of different structured glasses, together with flat glass and a commercial PV glass with AR coating.

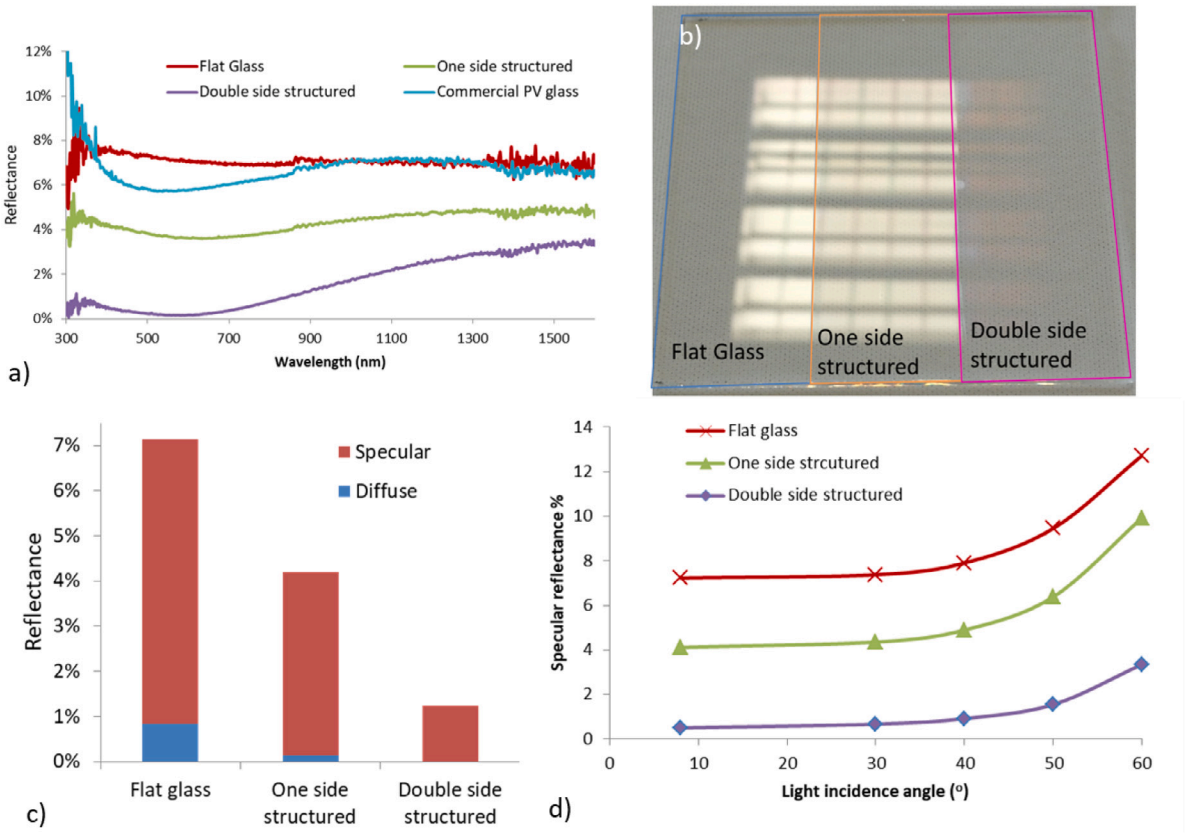

Fig. 6. Reflectance measurements. (a) Global spectral reflectance of one side structured glass, double side structured glass, flat glass and PV glass with AR coating. (b) Photograph of a glass sample reflection with three different structured areas.(c) Average reflectance components in the wavelength range between 300 nm and 1200 nm. (d) Specular reflectance for different light incident angles.

the glass, the reflectance decreased up to 6.2% in this spectral region, reflecting 1.0% in average, showing the potential of these structures to other applications related with light transmittance. This improvement in the AR performance can be visually appreciated in Fig. 6(b), where the reflection from ceiling lights from a flat glass, one side structured glass, and double side structured glass is shown.

Due to their small size, in comparison to the investigated wavelength region, the fabricated SWSs did not scatter light in this spectral range. To quantify this behaviour, the components of the global reflected light have been obtained. To this aim, the global and diffuse reflectances were measured, while the specular component was obtained from their subtraction. Fig. 6(c) shows the specular and diffuse reflectance averaged from 300 nm to 1200 nm for flat glass, one side and double side structured glasses. It can be seen that all cases, specular reflectance component clearly dominates, besides, specular and diffuse decreased for one side and double side structured glasses. The specular

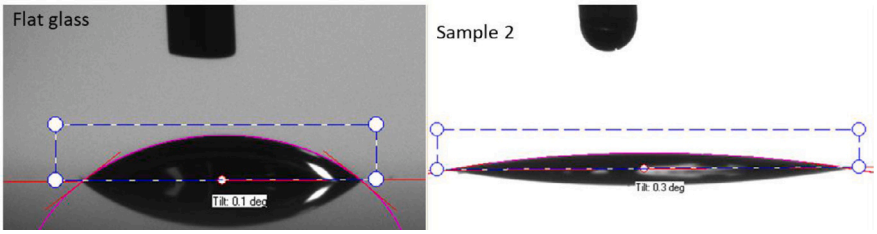

Fig. 7. Comparison of the water contact angle of flat glass and structured glasses.

component has notably decreased, from 6.3% until approximately 4.0% for one side structured glass and to 1.2% for double side structured glass. Similarly, the diffuse component has decreased too, from 0.8% to 0.5% for one side structured glass and less than 0.1% for double side structured glass.

Finally, to obtain the reflectance with respect to the light's angle of incidence, the specular reflectance was measured at different angles (8°, 30°, 40°, 50°, and 60°). The results are depicted in Fig. 6(d), where structured glasses showed an improved directional performance. One side structured glass reduced the reflectance up to 2.8%, and double side structured glass by 9.4% with respect to the flat glass at 60° of light incident angle. Double side structured glass shows an improved angle response in comparison to commercial nano-porous SiO_2 AR coatings, where for a light incidence angle of 60°, the difference between commercial non-coated glass and double-side coated glass was 7.6% absolute [34].

3.2. Wettability enhancement

In environments with high soiling rates like deserts, the electrical output of PV technology can decrease up to 50% [9]. To overcome this problem, wettability enhanced coatings can be added to PV cover glasses, modifying the surface energy by making it super-hydrophilic or super-hydrophobic. Super-hydrophobic surfaces are characterized by water contact angle (WCA), of static water droplets, higher than 150°. Mimicking the lotus leaf behaviour, water droplets are repelled from the surface becoming spherical in shape and they roll off quickly due to the low adhesion forces to the surface. In this way, the water droplets carry with them dust and soiling particles away and hence cleaning the panel. Conversely, super-hydrophilic surfaces present WCA below 10°. In this scenario, water droplets are spread over the surface forming a thin film where dust particles are picked up by water and washed away. Both behaviours allow to glass to clean itself and there is not yet a consensus regarding which of them provides better performance [9].

The well-regarded Young's equation, $\gamma_{sg} = \gamma_{sl} + \gamma_{lg}\cos\theta_Y$, describes the behaviour of an ideal smooth and homogeneous material in thermodynamic equilibrium, where θ_Y is Young's contact angle and γ_{sg}, γ_{sl} and γ_{lg} are the interfacial surface tensions of solid–gas, solid–liquid, and liquid–gas respectively that depend on the materials' free energy. In a non-ideal surface, Cassie–Baxter and Wenzel are the two main models that describe the wettability of rough surfaces. Both models attempt to relate the WCA of an ideal smooth surface (Young's angle, θ_Y) with the apparent one (θ^*): Wenzel model ($\cos\theta^* = r\cos\theta_Y$) and Cassie–Baxter model ($\cos\theta^* = r_f f\cos\theta_Y + f - 1$), where ($r$) is the roughness. According to these equations, the wettability of any surface can be modified by changing the surface free energy or by increasing the roughness of the surface [35].

The first modification can be done by adding chemicals to the surface, modifying the nature of it. On the other hand, by increasing the roughness, the behaviour of the material towards water is maximized. In our case, flat glass presented a moderate hydrophilic behaviour, with WCA of approximately 41°, but with the SWSs the surface wettability increased, showing an enhanced hydrophilic (Fig. 7). Table 2 shows the measured WCA and standard deviation of the measurements of the flat glass and structured glass.

Table 2
Topological parameters of structured glass samples.

	Flat glass	Structured glass
WCA (°)	40.8	11.5
σ	5.8	1.3

The difference between flat glass and structured glass is noticed, as the structured glass presented lower WCA (Table 2), providing to the glass an anti-fogging property. Fig. 8 shows the flat glass and the structured glass after being subjected to the deposition of water droplets. As can be seen from this figure, the structured glass did not fog due to its highly-hydrophilic property unlike flat glass, which was covered by fog.

However, just with the static contact angle the relation of the water behaviour on glass sample cannot be fully characterized. In order to obtain complementary information, the angle at with a DI-water droplet starts sliding, also known as roll-off angle (ROA), has also been measured. This parameter is related to the tendency of water to roll off the surface, carrying dust along the way in this manner. Ideally, this parameter should be less than the tilt angle of the solar panel. For this characterization, half of a 70 × 70 mm^2 glass sample has been structured, the other half corresponding to flat glass. After, red-tinted 20 μL of DI water was deposited on each surface, and the sample was manually inclined. At nearly 10° the water droplet on the structured side has started to roll off while more than 70° inclination were necessary for the droplet to start sliding (Fig. 9). In this way, PV modules laminated with these glasses, would have a self-cleaning effect, when installed at tilt angle higher than 10°.

3.3. Anti-soiling

These highly-hydrophilic surfaces can be easily cleaned by rain, fog, or even dew. However, in many regions where solar resource is more abundant, water availability is typically scarce [36], making this cleaning process an unfavourable mitigation approach. In fact, these locations have a high soiling rate and the need for cleaning is even greater. For this reason, WE coatings might also present anti-soiling behaviour. A strategy to provide this function relies on increasing the roughness of the surface [17,37–39]. In our study, SWSs increase the mean distance and the contact area between the dust/soil particle and the glass surface, decreasing therefore adhesion forces such Van der Waals and capillary ones [17,38,40]. To characterize this surface feature, a procedure has been developed which includes a soiling method and three characterization procedures including soiling weight, light transmission variation, and surface coverage as was described in Section 2 (Fig. 10).

The adhesion percentage, defined in Eq. (1), is an important parameter since it provides the relation between the deposited dust and the amount of it that has been adhered to sample surfaces. As it can be seen from Fig. 10, for flat glass, more than 80% of the deposited dust was adhered to its surface. In comparison, for the structured glass, only 37% of the deposited dust was adhered to the surface, showing a decrease of more than 55% in the soiling ratio.

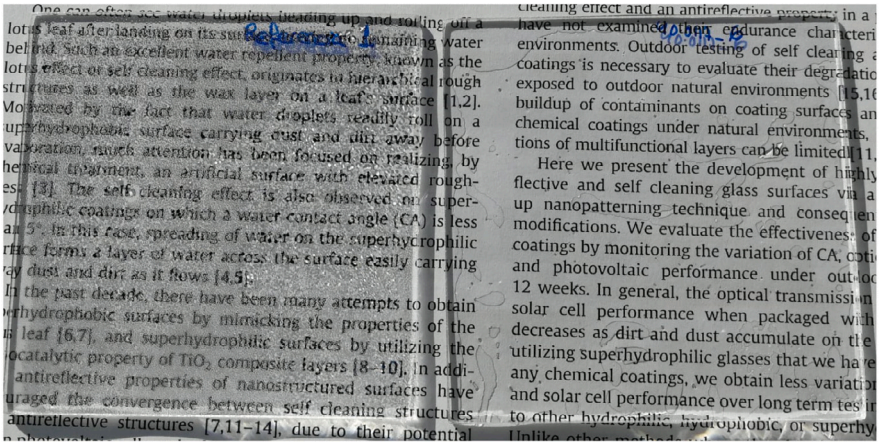

Fig. 8. Picture of two glasses showing the anti-fogging behaviour of the structured glass in comparison to flat glass.

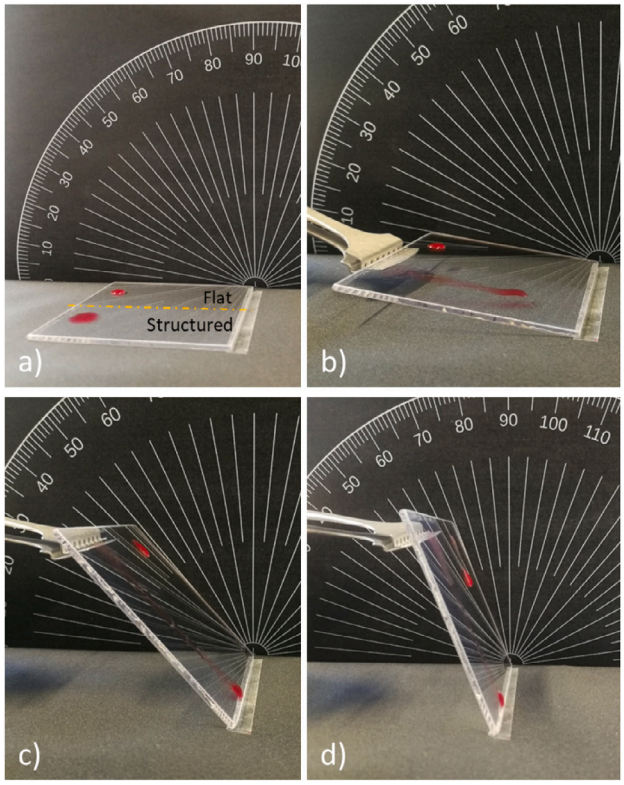

Fig. 9. Sequence images of water droplets in half–half structured and flat glass sample. (a) Glass sample at 0° with two water droplets. (b) Angle at where the droplets in structured size starts to fall (~10°). (c) Angle where the droplet on the flat glass is still in the start position (~50°). (d) Angle at where the droplet on the flat side starts to fall (~70°). For clarity, the drops have been stained with water-based red dye, nevertheless the experiment has also been performed without any dye showing same results.

Regarding the transmittance reduction, the tendency is kept. For soiled flat glass, the transmittance was reduced by more than 15%, in opposition to structured glass, for which it was only reduced by 7.8%, meaning a decrease of 48% in the soiling ratio.

The decrease in the transmission is closely related to the surface coverage. In the soiled flat glass, the dust covered the 48.4% of the total surface unlike the structured glass, where the coverage has been only 18.6%. The soiling ratio decreases slightly more than 60%.

In summary, applying different characterization methods, the soiling rate decreased from 60% to 48% using structured glasses.

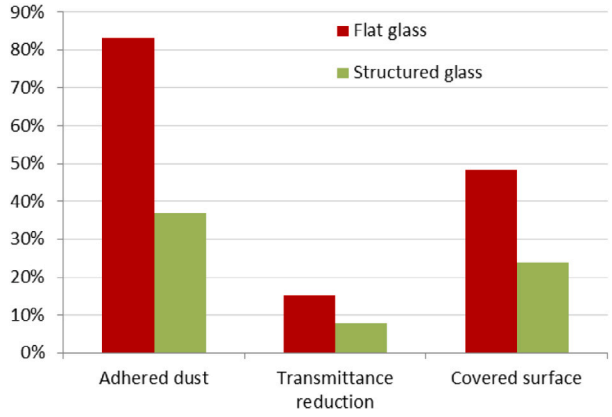

Fig. 10. Characterization of flat and structured glasses after the soiling procedure.

From the previous data, one can conclude that the structured glasses reduced to a half the decrease in the transmission and the coverage of the surface was even less (51% less in transmittance and 38% less in surface coverage). Therefore, this improvement in the anti-soiling behaviour could reduce the need of cleaning the modules, thus reducing the maintenance costs.

3.4. Lamination of solar cells

Once the structured glasses were completely characterized, the demonstration of their applicability to solar PV technology has been carried out. The glass structured with the optima nano-structures has been used as a front cover of one-cell solar PV module (mini-module MM). PERC solar cells have been laminated with flat glass and structured glass and their optical and electrical properties have been measured in the standard configuration: glass/EVA/Solar Cell/EVA/backsheet. The laminated solar cells are presented in Fig. 11 where it can be clearly seen that the reflection of the light abruptly decreases in the structured glass.

3.4.1. Electrical characterization

In order to test the influence of the structured glass on the mini-module performance, their electrical parameters have been measured using a calibrated flash solar simulator. The IV curve has been obtained in standard conditions (Fig. 12) and from this graph, the main electrical parameters have been compiled in Table 3. The electrical measurements uncertainties have been estimated taking into account the individual uncertainties of the calibrated equipments used for the

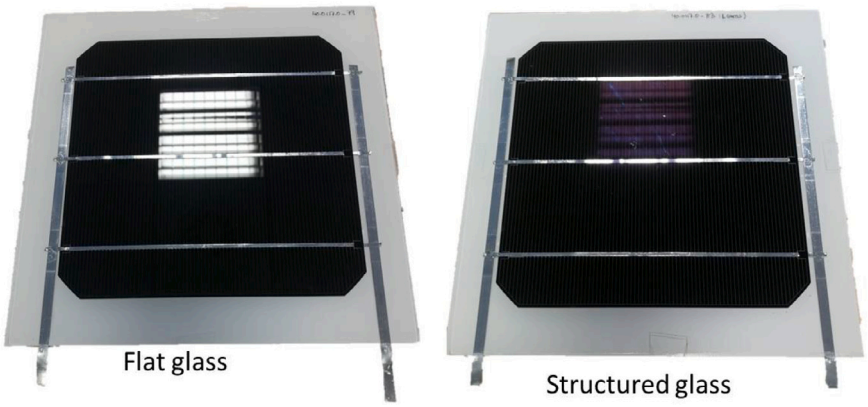

Fig. 11. Photographs of mini-modules laminated with flat glass and structured glass, where the reduction in reflection can be clearly noticed.

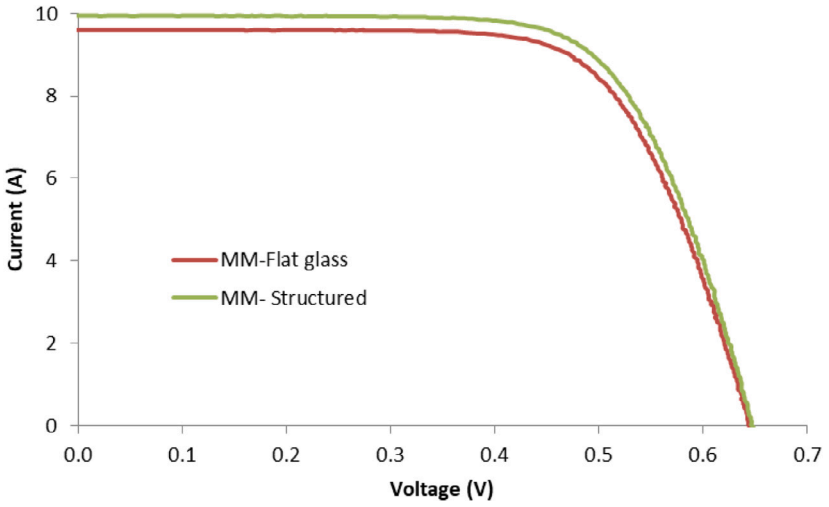

Fig. 12. Comparison of IV curve of mini-modules laminated with flat and structured glasses.

Table 3
Mini-modules' electrical parameters.

	I_{sc} (A) ±2.4%	V_{oc} (V) ±1.2%	I_{mp} (A) ±1.7%	V_{mp} (V) ±1.7%	P_{max} (W) ±2.7%	Fill Factor (%) ±0.7%
Flat glass	9.60	0.64	8.81	0.48	4.25	68.8%
Structured glass	9.94	0.65	9.12	0.49	4.45	69.1%

measurements. These uncertainties correspond to the expanded uncertainty obtained multiplying the standard uncertainty by the coverage factor $k = 2$ which corresponds to a confidence level of about 95%.

The structured glass improve the electrical performance of the photovoltaic mini-module as can be understood from Fig. 12 and Table 3. For the device laminated with flat glass, a short circuit current of 9.60 A was obtained. This value increased up to 9.94 A for device laminated with structured glass, providing a relative improvement of 3.5%. On the other hand, the fill factor showed a very small impact. The open circuit voltage remains approximately constant for both mini-modules, as expected.

3.4.2. Spectral response measurements

To complete the electrical characterization of these PV mini-modules, their spectral response has been measured (Fig. 13). As can be seen from Fig. 13, the sample laminated with structured glass showed a higher spectral response up to approximately 900 nm, which is translated in an improvement of 2.5% in the short circuit current density.

3.4.3. IAM factor measurements

The electrical production of a PV module depends, among many other parameters, on the light incident angle. This incident angle impacts on the amount of light transmitted throughout the glass front cover to the solar cell. As the light angle of incidence increases, more light gets reflected in this front cover glass. The ratio of the light absorbed by the solar module at some incident angle with respect to the light absorbed at normal incidence is known as the Incidence Angle Modifier (IAM) (2). A reliable determination of the IAM factor can be extremely helpful for an accurate estimation of the electrical production of tilt-fixed PV systems (i.e. building integrated PV) [41].

With the set-up described in the Materials and Methods section, the Isc (obtained from the I/V curve) has been measured from normal incidence, i.e. 0° up to 85°, with 5° step, and these values have been

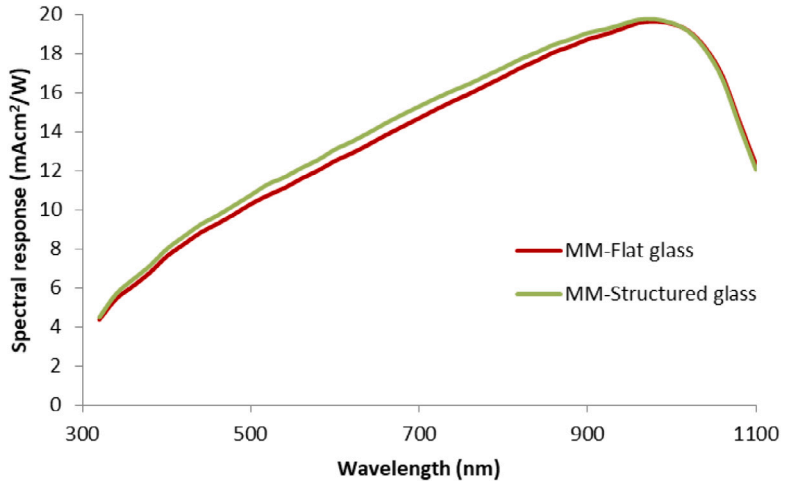

Fig. 13. Spectral response of the mini-modules laminated with flat glass and structured glass.

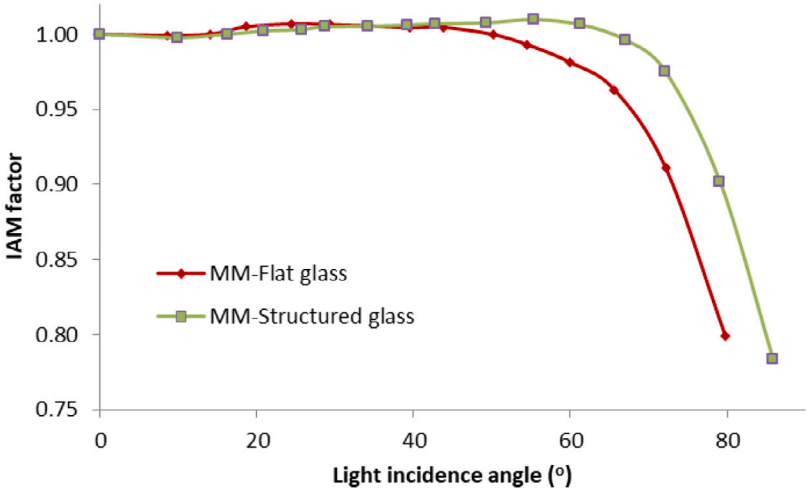

Fig. 14. Measurements of IAM factor of mini-modules laminated with flat and structured glasses.

normalized to the 0° incidence Isc value. The results are depicted in Fig. 14, where the mini-module laminated with structured glass showed an appreciable enhancement of the IAM factor above approximately 60°. According to these results, for 80° of incident angle, the mini-module laminated with structured glass showed an IAM factor of 0.9, and the mini-module laminated with flat glass presented an IAM factor of 0.80.

As a summary, Table 4 shows all the values of the different tests carried out to characterize the glass samples and the mini-modules (MM) laminated with these glasses.

4. Conclusions

We demonstrated that glass samples patterned by sub-wavelength random nano-cones made by a simple single-step self-masking RIE process can functionalize the glass providing omnidirectional anti-reflective (1%), super-hydrophilicity, and anti-soiling properties. These random nanostructures enhance the transmittance and wettability and reduce the amount of soiling particles adhered to the glass surface. In this work, special effort has been dedicated to quantify the impact of these properties in terms of PV module performance improvement. To this aim, spectral optical measurements have been carried out. A decrease of 6.1% ± 0.5% absolute in reflectance with respect to flat glass has been obtained for a double-side structured sample averaged from 300 nm to 1200 nm. With respect to the wettability property, these structured glasses present an enhanced hydrophilic behaviour (WCA = 11.53°), giving an additional anti-fogging property. Additionally, their sliding angle is significantly lower than the one for a flat glass, ~10° for structured glass and ~70° for flat glass respectively. Furthermore, the anti-soiling characteristic has been quantitatively analysed through three methods: dust adhesion, transmittance reduction, and surface coverage. In all three tests, structured glasses have presented an anti-soiling behaviour with respect to the flat glass (reduction of soiling ratio of 55% in dust adhesion, reduction of the soiling ratio of 60% in transmittance and reduction of soiling ratio of 48% in covered surface).

After the whole glass characterization, the structured glass sample and the flat glass have been used as a front cover of solar PV mini-modules. Their I–V curve, spectral response, and IAM factor has been measured. In all experiments, MM with structured glass has shown the best performance. The short circuit current increased from 9.60 A for the device laminated with the flat glass up to 9.94 A of the MM structured glass, representing a relative increase of 3.5%. With these enhancements, the fill-factor has increased up to 69.1%. The enhancement in the optical performance has been reflected in the spectral response measurements, where structured glass provided the PV device with highest values in the whole solar cells spectral region. Finally, the IAM factor has been measured, and a clear improvement

Table 4
Summary of the main parameters.

Properties	Flat glass	One side structured glass	Double side structured glass
Transmittance (±0.5%)	92.7	95.4	98.3
Reflectance (±0.5%)	7.1	4.1	1.0
		MM Flat Glass	MM Structured Glass
Anti-soiling	Transmittance reduction (±0.5%)	15.3	7.8
	Surface coverage (%)	48.4	24
	Adhered dust (%)	83.1	37
Wettability (WCA °)		40.8	11.5
Roll off angle (°)		~70	~10
Electrical characterization	Isc (A) ± 2.4%	9.60	9.94
	Imp (A) ± 1.7%	8.81	9.12
	Pmp (W) ± 2.7%	4.25	4.45
	FF (%) ± 0.7%	68.7	69.0
IAM factor (@ 80°)		0.80	0.88

has been obtained with the structured glass sample, obtaining a relative increase of more than 7.5% at light angle of incidence of 70° . With the obtained results, it can be concluded that solar PV devices laminated with subwavelength random nano-cones structured glasses enhance their performance, improving the electricity production thanks to its omnidirectional anti-reflective property and also decreasing the O&M cost, thanks to its anti-soiling function.

CRediT authorship contribution statement

Cristina L. Pinto: Methodology, Investigation, Writing – review & editing. **Iñaki Cornago:** Conceptualization, Methodology, Investigation, Writing – review & editing, Supervision. **Alicia Buceta:** Investigation. **Eugenia Zugasti:** Conceptualization, Investigation. **Jaione Bengoechea:** Conceptualization, Methodology, Writing – review & editing, Supervision.

Declaration of competing interest

The authors declare that they have no known competing financial interests or personal relationships that could have appeared to influence the work reported in this paper.

Data availability

The data that has been used is confidential.

Acknowledgements

Authors want to thank Adrián Vicente Gómara, from the Engineering Department of the Public University of Navarra for the WCA measurements, and Mikel Ezker for his help in the Isc, IAM factor, and spectral response measurements carried out in the flash simulator and the spectral response system.

Cristina Pinto gratefully acknowledges the Department of University, Innovation and Digital Transformation of the Government of Navarra for the grant for hiring doctoral students and doctoral students by companies, research centres, and technology centres: Industrial Doctorates 2020, with file number 0011-1408-2020-000003, received to carry out this study.

In the same way, Cristina thanks for the open access funding provided by Universidad Pública de Navarra.

References

[1] I. PVPS Task, Snapshot of Global PV Markets - 2020, Tech. Rep., 2021, URL www.iea-pvps.org.

[2] F.I.F.S.E. Systems, Photovoltaics Report, Tech. Rep., (July) Fraunhoger ISE, Freiburg, 2021, URL https://www.ise.fraunhofer.de/content/dam/ise/de/documents/publications/studies/Photovoltaics-Report.pdf.

[3] N. Shanmugam, R. Pugazhendhi, R. Madurai Elavarasan, P. Kasiviswanathan, N. Das, Anti-reflective coating materials: a holistic review from PV perspective, Energies 13 (10) (2020) 2631.

[4] V.P. Equipment, International technology roadmap for photovoltaic (ITRPV), 2021, September.

[5] H.A. Macleod, Thin-Film Optical Filters, CRC Press, 2010.

[6] D.B. Mahadik, R.V. Lakshmi, H.C. Barshilia, High performance single layer nano-porous antireflection coatings on glass by sol-gel process for solar energy applications, Sol. Energy Mater. Sol. Cells 140 (2015) 61–68, URL http://dx.doi.org/10.1016/j.solmat.2015.03.023.

[7] D. Chen, Anti-reflection (AR) coatings made by sol-gel processes: a review, Sol. Energy Mater. Sol. Cells 68 (3–4) (2001) 313–336.

[8] H.K. Raut, V.A. Ganesh, A.S. Nair, S. Ramakrishna, Anti-reflective coatings: A critical, in-depth review, Energy Environ. Sci. 4 (10) (2011) 3779–3804.

[9] A.S. Sarkın, N. Ekren, Ş. Sağlam, A review of anti-reflection and self-cleaning coatings on photovoltaic panels, Sol. Energy 199 (2020) 63–73.

[10] N. Cherupurakal, M.S. Mozumder, A.H.I. Mourad, S. Lalwani, Recent advances in superhydrophobic polymers for antireflective self-cleaning solar panels, Renew. Sustain. Energy Rev. 151 (2021) 111538.

[11] H. Qasem, Effect of Accumulated Dust on the Performance of Photovoltaic Modules (Ph.D. thesis), Loughborough University, 2013, URL https://dspace.lboro.ac.uk/2134/11735.

[12] T. Sarver, A. Al-Qaraghuli, L.L. Kazmerski, A comprehensive review of the impact of dust on the use of solar energy: History, investigations, results, literature, and mitigation approaches, Renew. Sustain. Energy Rev. 22 (2013) URL http://dx.doi.org/10.1016/j.rser.2012.12.065.

[13] A. Rao, R. Pillai, M. Mani, P. Ramamurthy, Influence of dust deposition on photovoltaic panel performance, Energy Procedia 54 (2014) 690–700, URL http://dx.doi.org/10.1016/j.egypro.2014.07.310.

[14] F. Mejia, J. Kleissl, J.L. Bosch, The effect of dust on solar photovoltaic systems, Energy Procedia 49 (2014) 2370–2376, URL http://dx.doi.org/10.1016/j.egypro.2014.03.251.

[15] M. Gostein, T. Duster, C. Thuman, Accurately measuring PV soiling losses with soiling station employing module power measurements, in: 2015 IEEE 42nd Photovoltaic Specialist Conference, PVSC 2015, (November) 2015, pp. 3–7.

[16] L.L. Kazmerski, M. Al Jardan, Y. Al Jnoobi, Y. Al Shaya, J.J. John, Ashes to ashes, dust to dust: Averting a potential showstopper for solar photovoltaics, in: 2014 IEEE 40th Photovoltaic Specialist Conference, PVSC 2014, 2014, pp. 187–192.

[17] H.R. Moutinho, C.S. Jiang, B. To, C. Perkins, M. Muller, M.M. Al-Jassim, L. Simpson, Adhesion mechanisms on solar glass: Effects of relative humidity, surface roughness, and particle shape and size, Sol. Energy Mater. Sol. Cells 172 (2017) 145–153.

[18] M.R. Maghami, H. Hizam, C. Gomes, M.A. Radzi, M.I. Rezadad, S. Hajighorbani, Power loss due to soiling on solar panel: A review, Renew. Sustain. Energy Rev. 59 (2016) 1307–1316.

[19] S. Wilson, M. Hutley, The optical properties of 'moth eye' antireflection surfaces, Optica Acta Int. J. Opt. 29 (7) (1982) 993–1009.

[20] B.M. Phillips, P. Jiang, Biomimetic antireflection surfaces, Eng. Biomim. (2013) 305–331.

[21] S. Chattopadhyay, Y.F. Huang, Y.J. Jen, A. Ganguly, K.H. Chen, L.C. Chen, Anti-reflecting and photonic nanostructures, Mater. Sci. Eng. R Rep. 69 (1–3) (2010) 1–35, URL http://dx.doi.org/10.1016/j.mser.2010.04.001.

[22] W.-L. Min, B. Jiang, P. Jiang, Bioinspired self-cleaning antireflection coatings, Adv. Mater. 20 (2008) 3914–3918, URL www.advmat.de.

[23] S. Nishimoto, B. Bhushan, Bioinspired self-cleaning surfaces with superhydrophobicity, superoleophobicity, and superhydrophilicity, RSC Adv. 3 (3) (2013) 671–690.

[24] Z. Han, Z. Jiao, S. Niu, L. Ren, Ascendant bioinspired antireflective materials: Opportunities and challenges coexist, Prog. Mater. Sci. 103 (2019) 1–68, URL https://www.sciencedirect.com/science/article/pii/S0079642519300118.

[25] R.H. Siddique, G. Gomard, H. Hölscher, The role of random nanostructures for the omnidirectional anti-reflection properties of the glasswing butterfly, Nature Commun. 6 (1) (2015) 1–8.

[26] J. Son, S. Kundu, L.K. Verma, M. Sakhuja, A.J. Danner, C.S. Bhatia, H. Yang, A practical superhydrophilic self cleaning and antireflective surface for outdoor photovoltaic applications, Sol. Energy Mater. Sol. Cells 98 (2012) 46–51, URL http://dx.doi.org/10.1016/j.solmat.2011.10.011.

[27] L.K. Verma, M. Sakhuja, J. Son, A.J. Danner, H. Yang, H.C. Zeng, C.S. Bhatia, Self-cleaning and antireflective packaging glass for solar modules, Renew. Energy 36 (9) (2011) 2489–2493, URL http://dx.doi.org/10.1016/j.renene.2011.02.017.

[28] J. Son, L.K. Verma, A.J. Danner, C.S. Bhatia, H. Yang, Enhancement of optical transmission with random nanohole structures, Opt. Express 19 (S1) (2011) A35.

[29] J. Van De Groep, P. Spinelli, A. Polman, Single-step soft-imprinted large-area nanopatterned antireflection coating, Nano Lett. 15 (2015) 4223–4228, URL https://pubs.acs.org/sharingguidelines.

[30] J.M. Newkirk, I. Nayshevsky, A. Sinha, A.M. Law, Q.F. Xu, B. To, P.F. Ndione, L.T. Schelhas, J.M. Walls, A.M. Lyons, D.C. Miller, Artificial linear brush abrasion of coatings for photovoltaic module first-surfaces, Sol. Energy Mater. Sol. Cells 219 (2021) 110757.

[31] M.Z. Khan, C. Pfau, M. Schak, P.-T. Miclea, V. Naumann, A. Debess, C. Hagendorf, K. Ilse, Resilience of industrial PV module glass coatings to cleaning processes, J. Renew. Sustain. Energy 12 (5) (2020) 053504, URL http://aip.scitation.org/doi/10.1063/5.0024452.

[32] C.L. Pinto, I. Cornago, A. Buceta, E. Zugasti, J. Bengoechea, Parametric analysis of random subwavelength structures with anti-reflective properties on glass applied to photovoltaics, Sol. Energy Mater. Sol. Cells 236 (2022) 111506, URL https://linkinghub.elsevier.com/retrieve/pii/S0927024821005432.

[33] International Electrotechnical Commission, International Standard IEC 61853-2. Vol. 2003, 61010-1 © Iec:2001, 2003, p. 13.

[34] X.-l. Wang, Anti-Reflective Coating on PV Cover Glass, PV Taiwan Forum, DSM Bright Science. Brighter Living, 2014.

[35] L.K. Verma, M. Sakhuja, J. Son, A. Danner, H. Yang, H. Zeng, C. Bhatia, Self-cleaning and antireflective packaging glass for solar modules, Renew. Energy 36 (9) (2011) 2489–2493.

[36] European Commission, Communication from the Commission to the European Parliament, the Council, the European Economic and Social committee and the Committee of the Regions Roadmap to a Resource Efficient Europe, Tech. Rep., European Comission, Brussels, 2011, pp. 1–25, URL https://eur-lex.europa.eu/legal-content/EN/TXT/PDF/?uri=CELEX:52011DC0571{&}from=EN.

[37] E. Klimm, T. Kaltenbach, D. Philipp, M. Masche, K.-a. Weiss, M. Koehl, Soiling and abrasion testing of surfaces for solar energy systems adapted to extreme climatic conditions, in: European PV Solar Energy Conference and Exhivition, (September) Hamburg, Germany, 2015, pp. 1–3.

[38] S. You, M.P. Wan, Mathematical models for the van der waals force and capillary force between a rough particle and surface, Langmuir 29 (29) (2013) 9104–9117.

[39] R. Jones, H.M. Pollock, J.A. Cleaver, C.S. Hodges, Adhesion forces between glass and silicon surfaces in air studied by AFM: Effects of relative humidity, particle size, roughness, and surface treatment, Langmuir 18 (21) (2002) 8045–8055.

[40] Y.I. Rabinovich, J.J. Adler, M.S. Esayanur, A. Ata, R.K. Singh, B.M. Moudgil, Capillary forces between surfaces with nanoscale roughness, Adv. Colloid Interface Sci. 96 (1–3) (2002) 213–230.

[41] M. Ezker, J. Bengoechea, J.M. Cuadra, L. Casajus, A.R. Laguna, Determination of incidence angle modifiers for different photovoltaic, in: 31st European Photovoltaic Solar Energy Conference and Exhibition, Amsterdam, 2014, pp. 2822–2828.